https://doi.org/10.1007/s41230-025-4028-y

Simulation study on integrated bottom car body formation by high pressure die casting with a dual injection system

Rong Xiao[1], Jing-guo Wang[2], **Shao-xing Meng[3], Wei-dong Mao[1], Li-geng Yang[1], Jin Zhang[1], Lei Song[1], Wan-tong Chen[4], and *Wen-bo Yu[4]

1. Chery New Energy Automobile Co., Ltd., Wuhu 241000, Anhui, China

2. School of Materials Science and Engineering, Jilin University, Jilin 130022, China

3. Beijing Supreium Technology Co., Ltd., Beijing 100083, China

4. School of Mechanical and Electronic Control Engineering, Beijing Jiaotong Univerisity, Beijing 100044, China

Abstract: This study investigates the formation feasibility of the integrated bottom car body components with dual die casting injection molding technology. During the production of a die-cast super-large one-piece body part weighing over 10,000 t, a thorough comparison and investigation were conducted on the arising issues, using both single and double injection systems. Particular attention was given to meticulously discussing the die casting filling problems and microstructural defects that originated from the filling process. The research findings indicate that the implementation of a double injection system can significantly minimize cold shuts and reduce the solidification time. The effectiveness of this die casting technique was further confirmed by the production of high-quality castings using a scaled model that replicated real casting conditions at a 1:3 ratio, thereby maintaining a one-to-one correspondence in essential aspects. This successful study offers both theoretical insights and practical applications for the production of integrated bottom car bodies utilizing die casting in conjunction with a dual injection system.

Keywords: intergrated bottom car body die casting (megacasting); dual injection system; scaled model; die casting filling problems

CLC numbers: TP391.9 **Document code:** A **Article ID:** 1672-6421(2025)04-363-11

1 Introduction

Aluminum alloys are wildly used in automobile industry due to its low weight and good anti-corrosion properties [1]. However, the current body structure is generally complicated in design for achieving the necessary stiffness and strength, which aroused the long processing time, high cost, and low efficiency [2]. Recently, as illustrated in Fig. 1, the appearance of the integrated die-casting technology supports one solution for resolving these problems through utilizing the large die-casting machines accompanied with the designed die. This approach successfully replaces the traditional multiple processes, which includes the riveting, stamping, and welding. Furthermore, this technology can strongly reduce the part weight and cut the costs [3-8]. Due to these advantages, the integrated die-casting technology is evolving towards to the higher integration and larger size [4]. For example, the 16,000 t die-casting machine equipped with a die over 200 t has been recently developed in China [9].

As die-casting machine capacities continue to increase, the production of large, integrated die-cast products encounters numerous challenges. These include extended filling time and greater metal flow distances during the die casting filling stage. Such conditions exacerbate issues such as cold shuts and compromised mechanical properties in areas distant from the gate [10, 11]. To resolve these issues, the multi-shot injection technology has emerged. In comparison to the single-shot injection casting system, the multi-shot systems can effectively shorten the metal flow length, which can

*Wen-bo Yu

Male, Ph. D., Professor. His research interests mainly focus on the high pressure die casting technology.

E-mail: wbyu@bjtu.edu.cn

**Shao-xing Meng

E-mail: sx.meng@supreium.com

Received: 2024-02-15; Revised: 2024-06-02; Accepted: 2024-07-29

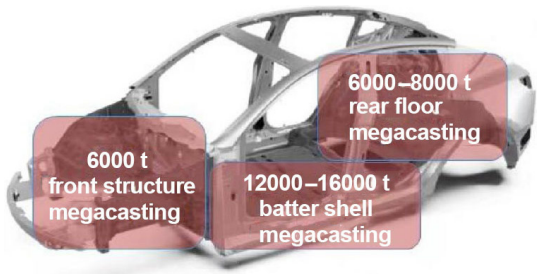

Fig. 1: Current application of integrated die-casting technology

reduce the filling time and keep the metal at a high temperature during the final filling stage. These advantages strongly reduce the appearance probability of cold shuts [12]. To produce a large integrated structural part, Tesla developed an innovative patent for a multi-shot system. This system consists of a fixed set of central dies and four movable mold sets [12]. Subsequently, several domestic automotive manufacturers and die-casting suppliers proposed the similar concepts. At the end of 2023, Chery and LK Tech jointly released the first dual-shot system with locking force over 10,000 tons [13], which significantly stimulates the practical application of multi-shot systems.

The dual-injection system, while offering significant advantages, does indeed pose several technical challenges that need to be carefully considered and addressed [5]. The high costs associated with die-casting machines and peripheral equipment, along with the complexities involved in designing die-casting dies, are notable hurdles. These factors have contributed to the relatively slow progress in implementing multi (dual) injection systems. Currently, the dual-injection system is still in its exploratory phase, lacking concrete product manufacturing trials and relevant literature to guide further development. Relevant technical solutions and research works are mainly focused on single-injection system solutions [7, 8, 10, 11]. Our research team has identified the following important research questions that need to be addressed in the development of dual-injection production processes: designing an effective gating system for dies specifically tailored to dual-injection processes, assessing whether die-casting machinery meets the stability standards necessary for dual-injection production, and analyzing the die-casting process and potential defects in large integrated parts produced through dual-injection.

This study employed a method combining simulation modeling with experimental validation to study the feasibility of dual injection die-casting for large integrated automotive body structures. This research encompassed three aspects: first, establishing a simulation model for the dual-shot system's filling process, conducting simulation verification, predicting the filling process, and analyzing the causes of defects; second, conducting dual-injection process experiments on a scaled-down model of an integrated automotive body, producing trial products for comparison with the simulation model to validate its accuracy, and optimizing the product gating system based on the scaled-down model's experiments; third, using the scaled-down model's experimental results to design the gating system for real products, performing calculations through simulation modeling to analyze the filling process and defect generation, and simultaneously conducting asynchronous analysis of the die-casting machine's injection control system to validate the feasibility of the integrated dual-shot system for forming automotive body structures.

2 Simulation modeling

The dual-shot simulation model in this study was based on the underlying CAE algorithm of SupreCAST developed independently by Beijing Supreium Technology Co., Ltd. [14–19]. To accurately simulate the filling process of the molten metal, the lattice Boltzmann method (LBM) was used as the fluid solution model. LBM is regarded as a mesoscopic fluid mechanics solving method. The large-scale parallel computing clusters can be relatively easily achieved, which makes it suitable for simulating the metal filling process of large integrated die casting products [20, 21]. In the context of integrated die-casting, compared to methods like FVM, LBM has the capability to use finer grid sizes and a greater number of grids to calculate the filling process of large-sized automotive casting parts. Additionally, during the high-speed filling stage where the molten metal is in a turbulent state, the multiple relaxation time (MRT) model was adopted to enhance the stability of the turbulence calculation process [21]. The free surface tracking of the molten metal was implemented using the volume of fluid (VOF) method, and the model is detailed in Section 2.1. For the filling process of the dual-shot system, a dual-plunger calculation model and an independent control scheme for the dual-plunger system were adopted. The model is elaborated in Section 2.2. The dimensions of the integrated body were in the range of 1.3 m×2.5 m and a thickness ranging from 3–5 mm. For this size, the traditional uniform grid partitioning method would generate the grids with a number in the order of billions. To resolve this problem, an adaptive grid architecture for grid partitioning of this large product was employed, and the grid model is detailed in Section 2.3.

2.1 LBM-VOF modeling

The LBM is based on the motion and collision of microscopic particles, employing a discrete velocity model to describe the distribution function of fluid particles. This makes LBM mathematically simpler than traditional Navier-Stokes (N-S) equations [18,22]. The model used in this work was divided into three parts: LBM principles, the multiple relaxation time (MRT) model, and the interface tracking model (VOF model).

2.1.1 Principles of LBM

Based on the Lattice Bhatnagar-Gross-Krook (LBGK) model, the LBM model is described as [22]:

$$f_i(\boldsymbol{x}+\boldsymbol{c}_i\Delta t, t+\Delta t) = f_i(\boldsymbol{x},t) + \Omega_i(\boldsymbol{x},t) \quad (1)$$

where i refers the ith discrete velocity directions, $\boldsymbol{x}$ refers spatial position coordinates, $\boldsymbol{c}_i$ refers ith discrete velocity components, t refers current moment, Δt refers time steps, $f_i(\boldsymbol{x}+\boldsymbol{c}_i\Delta t, t+\Delta t)$ and $f_i(\boldsymbol{x},t)$ refer the density distribution

function of position and time, respectively. $\Omega_i(\boldsymbol{x},t)$ is the collision term, derived from the LBGK approximation [22]:

$$\Omega_i(\boldsymbol{x},t)=\frac{f_i(\boldsymbol{x},t)-f_i^{\mathrm{eq}}(\boldsymbol{x},t)}{\tau}\Delta t \tag{2}$$

The equilibrium distribution function is defined as [22]:

$$f_i^{\mathrm{eq}}(\boldsymbol{x},t)=\omega_i\rho\left(1+\frac{\boldsymbol{u}\cdot\boldsymbol{c}_i}{c_s^2}+\frac{(\boldsymbol{u}\cdot\boldsymbol{c}_i)^2}{2c_s^4}-\frac{\boldsymbol{u}\cdot\boldsymbol{u}}{2c_s^2}\right) \tag{3}$$

where ω_i is the density weight in the ith discrete velocity direction, ρ is the density of the fluid, $\boldsymbol{u}$ is the fluid velocity at the current position and moment, c_s is the lattice sound velocity, and τ is the relaxation time.

The macroscopic field density ρ is given by [22]:

$$\rho(\boldsymbol{x},t)=\sum_i f_i(\boldsymbol{x},t) \tag{4}$$

The macroscopic field velocity $\boldsymbol{u}$ is given by [22]:

$$\boldsymbol{u}(\boldsymbol{x},t)=\frac{\sum_i \boldsymbol{c}_i f_i(\boldsymbol{x},t)}{\rho(\boldsymbol{x},t)} \tag{5}$$

2.1.2 MRT model

To address the flow problems associated with high Reynolds numbers during the filling process, this work employed the MRT model based on the LBGK model. The principle of the MRT model involves transforming the density space into the moment space by performing a matrix transformation on the distribution function. This transformation yields moments of different orders, where the zeroth-order moment of the distribution function represents the mass of each cell, the first-order moment represents the momentum of each cell, and so forth. Subsequently, collisions were applied to these moment variables, and the resulting moments were transformed back into the distribution function for the next step through the inverse matrix operation. The specific mathematical description is detailed as follows [22]:

$$f_i(\boldsymbol{x}+\boldsymbol{c}_i\Delta t,t+\Delta t)-f_i(\boldsymbol{x},t)=-M^{-1}SM[f_i(\boldsymbol{x},t)-f_i^{\mathrm{eq}}(\boldsymbol{x},t)]\Delta t \tag{6}$$

where M is the transformation matrix [21], and S is the relaxation matrix [22].

$$S=\mathrm{diag}(0,\omega_e,\omega_\varepsilon,0,\omega_q,\omega_v,\omega_v,\omega_\pi,\omega_v,\omega_v,\omega_v,\omega_m,\omega_m,\omega_m) \tag{7}$$

where ω_e, ω_ε, ω_q, ω_v, ω_π, and ω_m correspond to density, energy, energy squared, momentum, heat flux, and momentum flux relaxation rate, respectively.

2.1.3 VOF model

In this study, the VOF model [15] comprises three essential elements: the methodology for free surface distribution, the tracking technique, and the application of boundary conditions. In the VOF interface tracking within the MRT-LBM framework, specific interface functions are defined as [15]:

$$\frac{\partial\varepsilon}{\partial t}+\nabla\cdot(\boldsymbol{u}\varepsilon)=0 \tag{8}$$

where ε and $\boldsymbol{u}$ represent fluid fraction and velocity, respectively.

Equation (8) can be discretized by the control volume method [15]:

$$\varepsilon^{t+\Delta t}=\varepsilon^t-\Delta t\sum_{k=1}^{6}\varepsilon_k\boldsymbol{u}_k\boldsymbol{n}_k \tag{9}$$

where $\boldsymbol{u}_k$, $\boldsymbol{n}_k$, and ε_k represent the fluid velocity, external normal vectors, and filling degree on the kth face, respectively. $\sum_{k=1}^{6}\varepsilon_k\boldsymbol{u}_k\boldsymbol{n}_k$ represents the mass flux between the six neighboring control volumes, as shown in Fig. 2, and can be further expressed as:

$$\sum_{k=1}^{6}\sum_{i=1}^{18}\varepsilon_k\boldsymbol{n}_k\cdot\left[\boldsymbol{e}_i f_i(\boldsymbol{x})+\boldsymbol{e}_i f(\boldsymbol{x}+\boldsymbol{e}_i)\right]/2 \tag{10}$$

where $\boldsymbol{e}_i$ represent the LBM lattice direction, $\boldsymbol{x}$ respresent location.

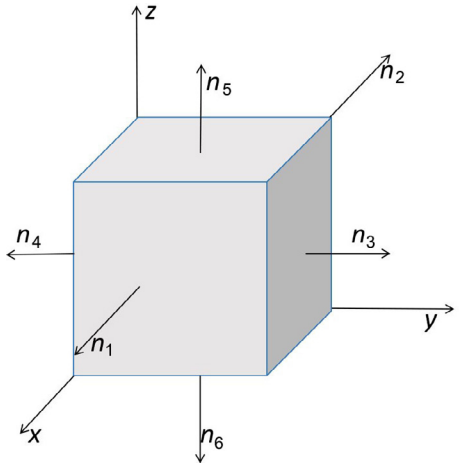

Fig. 2: Normal direction of the control volume

2.2 Simulation algorithm in dual injection system

In traditional die casting simulations, the users are typically allowed to set only one plunger. To meet the requirements of dual-shot simulations, this work generated the grids for the dual-plunger injection systems. The parameters of each injection system were independently configured, which enables to independently control each of the dual-shot systems. The differences in the dual injection control system of the die-casting machine were simulated, and thus the differences in metal liquid filling caused by the asynchronous problem of the die-casting machine were obtained. As shown in Fig. 3, the schematic diagram of temperature changes in molten metal under the dual injection system was illustrated.

A notable challenge in dual injection die-casting simulations is the large area of liquid metal hedging phenomena. To address this issue, a large eddy simulation (LES) model was developed to improve computational stability [23]. The LES method separates between large-scale and small-scale eddies by using a filtering function (related to mesh size). This approach offers more reliability compared to the traditional reynolds-averaged navier-stokes (RANS) method, especially when more detailed product shapes are depicted [23]. In the LBM framework, the LES model can dynamically adjust the relaxation time according to the spatial flow state.

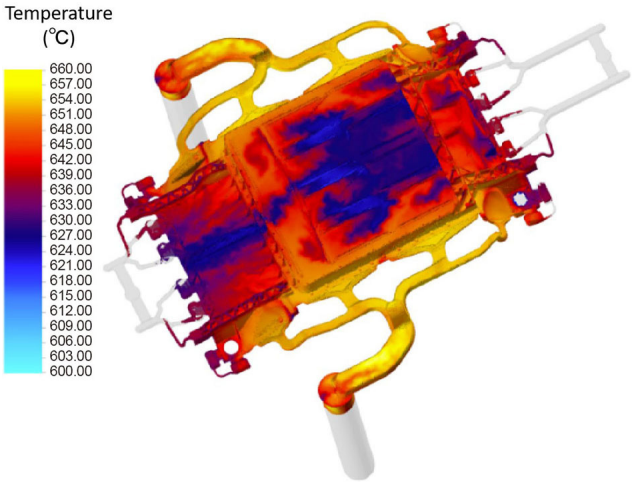

Fig. 3: Simulation results of temperature in molten metal under a dual injection system

2.3 Implementation of massively parallel computing based on block-structured AMR mesh

Integrated die-casting filling simulations often require over 100 million meshes, leading to substantial computational demands. To balance computational efficiency with accuracy, a block-structured adaptive mesh refinement (AMR) technique was utilized, which is based on the heterogeneous parallelism of GPU+CPU systems [24-26]. The 3D geometric model, depicted in Fig. 4, uses various mesh sizes at different layers to facilitate parallel resource allocation and dynamic mesh division. This method reduces the total mesh size while maintaining accuracy. The mesh sizes range from 1 mm to 8 mm, achieving a simulation scale of 400 million meshes.

Based on the above mesh refinement techniques, the computational domain was divided into multiple load-balanced cluster blocks. Each block's mesh cell was processed and computed by independent threads. Data exchange between cluster blocks was accomplished using MPI (+OpenMP), ensuring efficient parallel solving.

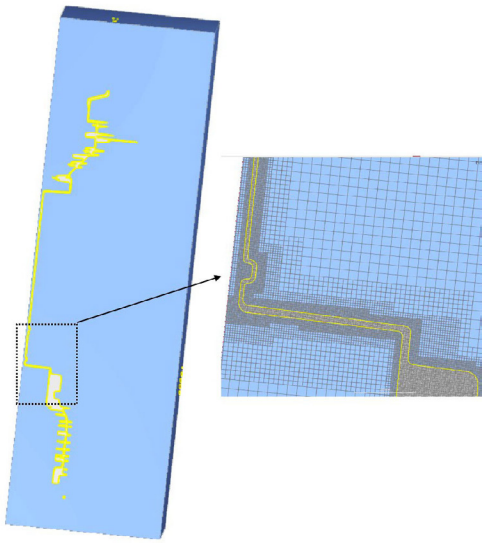

Fig. 4: AMR mesh based on block-structure

3 Die-casting parts and gating system

3.1 Die-casting products

As shown in Fig. 5, the integrated die-cast product of "Small Ant" bottom car body has a mass of 64 kg and is composed of the front compartment, battery lower shell, and rear floor. The integrated die-cast product of the "Small Ant" bottom car body consists of over 145 individual components and has overall dimensions of 2,500 mm×1,300 mm. The main wall thickness in the thin-wall region measures 5 mm and localized wall thickness is specified 3 mm.

3.2 Materials

An Al-Si alloy was chosen for production of this die-casting bottom car body, as Si element could enhance the fluidity of Al liquid. However, much more Si content leads to the reduction in elongation [27,28], which is harmful to the car body's operational requirements, including collision resistance and durability. Therefore, the non-heat-treated C891 alloy with Si content ranging between 7%–10% was chosen. The element composition and thermophysical properties are respectively given in Tables 1 and 2. The die material is H13 steel.

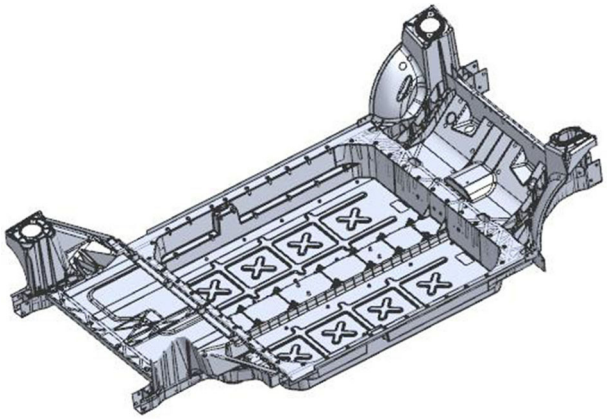

Fig. 5: One-piece bottom car body die-casting structure in "Small Ant"

Table 1: Chemical compositions of C891 alloy (wt.%)

Si	Fe	Mn	Mg	Ti	Others	Al
7.0–10.0	<0.2	0.4–1.0	0.2–0.7	<0.5	0.05–0.5	Bal.

Table 2: Thermophysical properties of C891 alloy

Density ($g·cm^{-3}$)	Conductivity [$W·(m·K)^{-1}$]	Solidification range (°C)	Specific heat capacity [$J·(kg·°C)^{-1}$]	Solidification latent heat ($kWh·kg^{-1}$)
2.67	135–170	600–510	$0.83×10^3$	0.12

3.3 Gating system and process parameters

Figure 6 illustrates the integrated die casting bottom car body with a dual injection system. The overall size of 2,725 mm×2,621 mm×645 mm and a wall thickness of 3 mm

surpasses the known maximum size of similar systems in current industry. Notably, it achieves a single-side filling distance of 860 mm. Given its application as the integrated battery shell, it is crucial to ensure the complete sealing of the battery bottom plate and prevent any gas entrapment during the filling process.

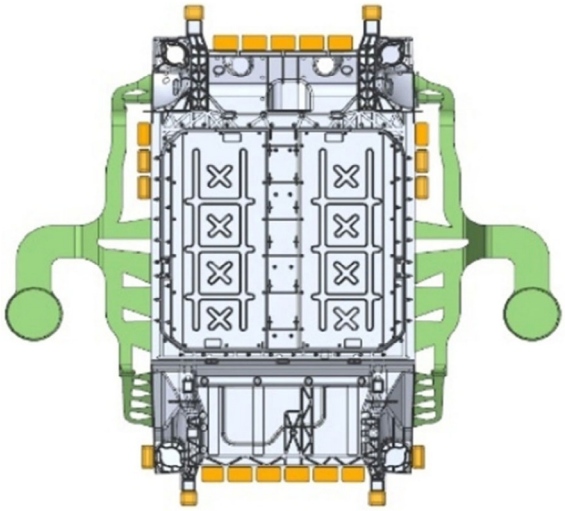

Fig. 6: Dual-injection gating systems in this work

To validate the feasibility of this dual injection gating system, a scaled model was designed for experimental and simulation comparison. As shown in Fig. 7, the scaled model is compressed to a 3:1 ratio. The external dimension is 840 mm×438 mm×220 mm, and its wall thickness is 1.3 mm. This dual injection scaled model firstly achieves an overall filling distance of 700 mm and a gating system weight of 8.3 kg. Table 3 presents the process parameters of the simulation.

The solid-liquid phase temperature range of the aluminum alloy is 510–600 °C, while the usual metal liquid temperature used in die casting is 620–720 °C [29]. Considering the weight of the casting, the initial filling temperature was set at 650 °C. To achieve the integrated car bodies with thin walls and high surface quality, the recommended filling speed was 25–30 $m \cdot s^{-1}$ [30]. The internal high-speed filling speed chosen for this experiment was 30 $m \cdot s^{-1}$. Based on the internal gate area and the die

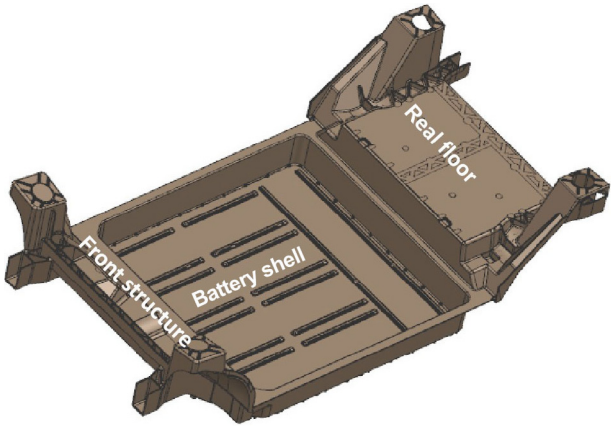

Fig. 7: 3D modeling of scaled casting

Table 3: Process parameters for scaled-model/cast flow analysis

Parameters	Values
Al liquid filling temperature (°C)	650
Slow punch speed ($m \cdot s^{-1}$)	0.2
High punch speed ($m \cdot s^{-1}$)	4.0
High filling speed of inner gate ($m \cdot s^{-1}$)	30
High speed start position (mm)	393
Al liquid filling time (ms)	50
Boost pressure (0.1 MPa)	160
Clamping force (t)	800
Punch diameter (mm)	90×2
Sleeve filling rate (%)	50
Sleeve initial temperature (°C)	150
Number of cycles	1
Inner gate area (mm^2)	989×2
Vacuum start position (mm)	100

diameter, the high injection speed was approximately 4.5 $m \cdot s^{-1}$. To prevent air entrapment, the slow injection speed of the die was set at 0.2 $m \cdot s^{-1}$. Based on the calculated high injection speed of the metal melt, the approximate cavity filling time for aluminum melt was around 50 ms. The high-speed stage was initiated when the metal melt filled the sprue, and the starting position of the high injection speed was at 393 mm. Additionally, the die-casting machine tonnage used in this scale-down experiment was 800 t.

4 Results and discussion

4.1 Comparison of experiment and simulation in the scaled casting

4.1.1 Flow state

The flow traces, as depicted in Fig. 8(a), were utilized to observe the flow state of the liquid metal as it transitioned from the double sleeve into the scaled model, revealing that the casting was completely filled with the liquid metal. The two streams firstly flow into the scaled model from different injection systems. Once the two liquid metal streams encounter, two streams converge along the *x*-direction and form the flow in the center of the battery cabin. This phenomenon is further confirmed by the simulation results. It is clear that the designed dual injection system can significantly reduce the flow length of the liquid metal. Once each of the dual injection systems fills their respective sides, the integrated two liquid metal flows proceed with the subsequent filling.

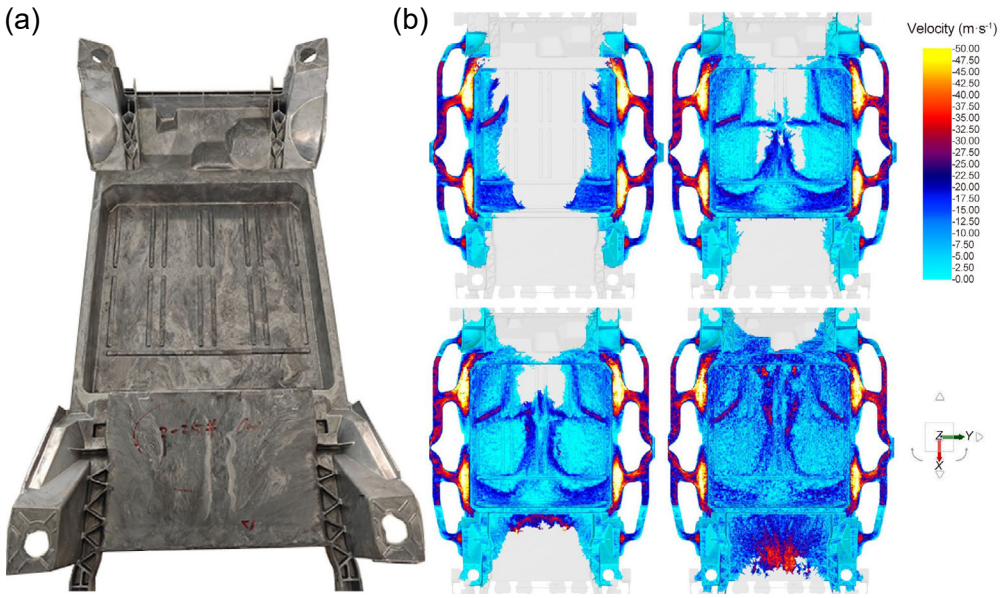

Fig. 8: Flow evolution of actual (a) and simulated (b) results of the scaled model

As indicated by the arrows in Fig. 9(a) in the rear floor plate (a critical zone of the component), the sequence and direction of the liquid metal flow can be seen from the patterns left by the release agent. The velocity field at the end of the filling can reach 30 $m \cdot s^{-1}$, as shown in Fig. 9(b). Before the merge of the two flows, each of them flows towards the crossbeam area with diagonal and vertical paths. Eventually, they incorporate together at the end of the rear floor plate.

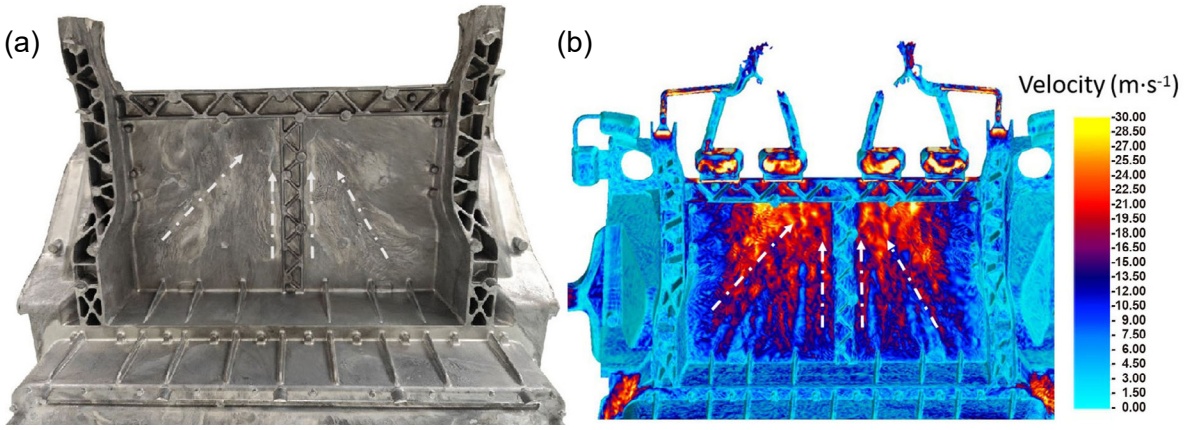

Fig. 9: Flow evolution of the rear floor plate: (a) actual; (b) simulated results

4.1.2 Defects

Figure 10(a) presents the defects including cold shuts and pore defects in the middle battery cabin of the scaled model. Their formation maybe caused by the incomplete gas removal and the low interfacial temperature of the front stream at the final stage. Collaborated with the simulation results shown in Fig. 10(b), it is clear that the pressure of the entrapped gas changes. During the filling process, the gas experiences compression, leading to an increased pressure within the central gas domain. The juncture of convergence between the two sides, where the gas eventually dissipates, corresponds to the location shown by the black circle in Fig. 10(a). Furthermore, Fig. 10(c) elucidates that the middle position of liquid metal in the flat plate is the region with low temperatures, which corresponds to the cold shuts position in products.

Figure 11(a) depicts the oxidized defects located at the rear floor plate. The oxidation positions are influenced by the surface impingement in the liquid metal. The simulation results presented in Figs. 11(b–c) reveal a significant correlation between the temperature distribution and gas content within the flow. Specifically, the regions of relatively low temperature align closely with areas where gas content is concentrated. This overlap is noteworthy as it corresponds to defects observed in the actual product.

Through the analysis of the flow traces and defects in the experiment and simulation results of scaled model, the flow range of each injection system is half of the area of the product in a dual injection system. This can significantly shorten the processing length. Two liquid metal flows then integrate and proceed with the subsequent filling process. Furthermore,

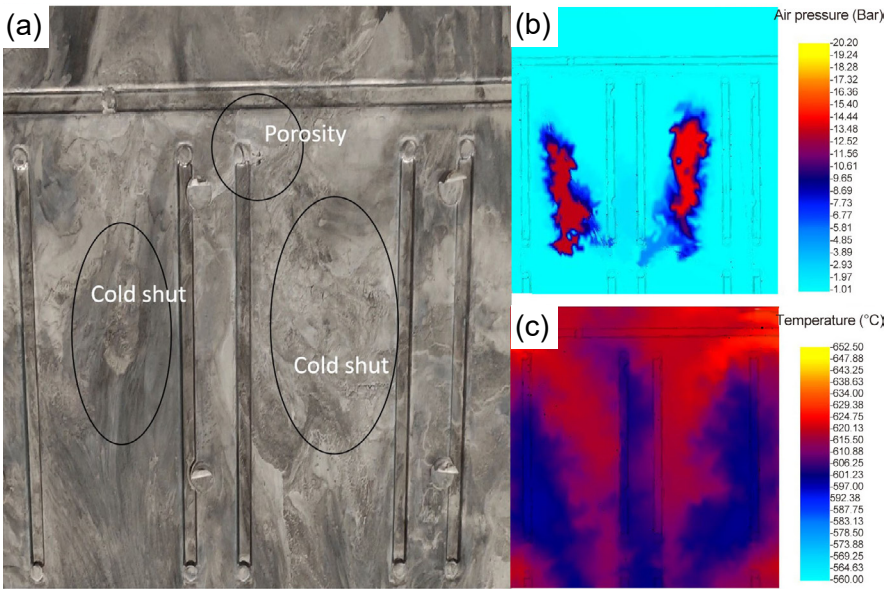

Fig. 10: Defects in the middle battery cabin of the scaled model: (a) actual defects; (b) simulated pore prediction; and (c) temperature field

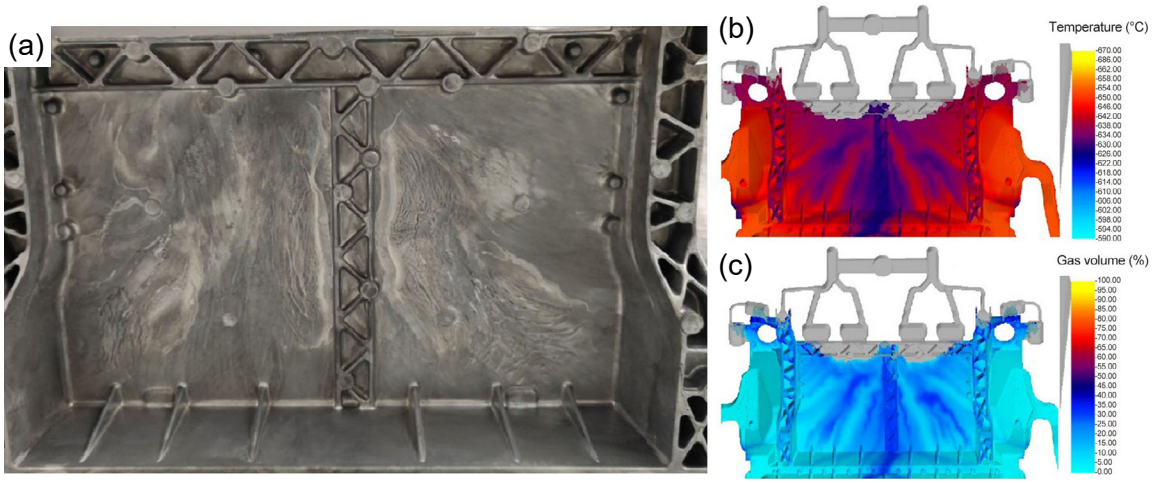

Fig. 11: Defects in the rear floor plate: (a) actual defects; (b) simulated temperature field and (c) gas content

the accuracy of the simulation was verified by scaled model experimental results, which provides a robust theoretical foundation for predicting the behavior of the actual production. It is noteworthy that defects identified in the scaled model can be solved in the real version by optimizing the runner design. Furthermore, as the actual product is 3 times larger than the scaled model, a significantly lower heat dissipation rate would occur. Consequently, the liquid metal with a higher temperature at the end of the filling state would help prevent the defects of cold shuts.

4.2 Analysis of simulation results in the actual casting

Based on the above discussion, this section evaluates the simulation results of the actual model. The simulation results include two parts. Firstly, it involves predicting potential defects such as convergence areas, pores, cold shut, and oxidation position. This analysis serves to optimize the gating procedure, aiming to ensure the production of qualified products. Secondly, due to the complexity introduced by the dual injection system of the die-casting machine, it assesses the machine's capability to meet the production demands, which is conducted from the perspectives of both synchronous and asynchronous.

4.2.1 Prediction of filling process and defects of actual product

Figure 12 illustrates that upon entering the product, the liquid metal from both sides of the gating system undergoes a high-speed filling stage. The flow sequence and filling process are similar to those observed in the scaled model, filling along with the x-direction. Differently, Figs. 12(a)–(d) demonstrate liquid metal sequentially drives gas toward the slag ladle. This ensures a methodical filling after convergence, effectively preventing the formation of pores within the product. The filling sequence predominantly extends from the central battery cabin towards the front cabin and rear floor plate areas.

As shown in Fig. 13(a), this ideal filling sequence leads to smoother removal of gases from the molten metal. Main oxidation areas concentrate at the forefront of the molten metal, and finally aggregates at the slag ladle. Figure 13(b) depicts the convergence area of the liquid metal, where the flow

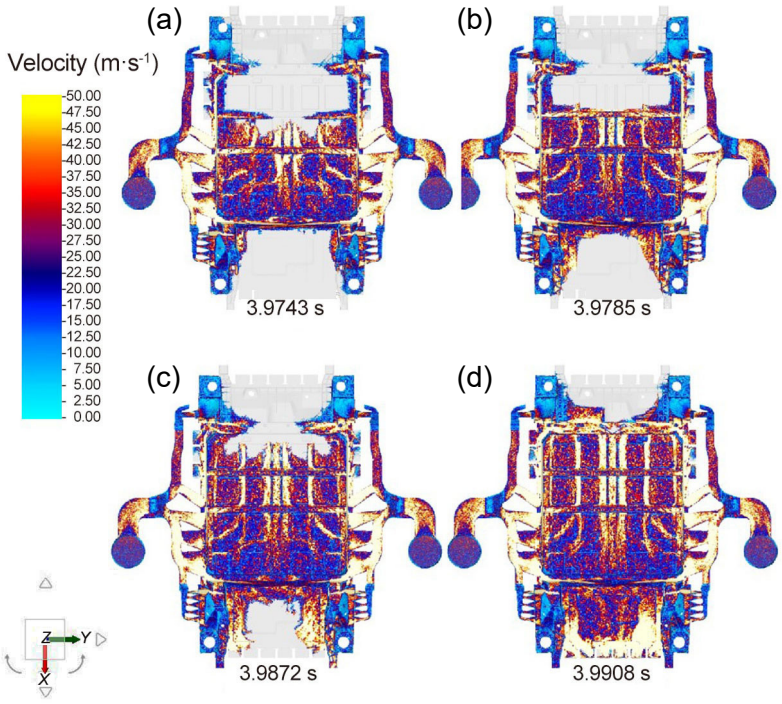

Fig. 12: Filling process of actual model: (a)–(d) velocity field distribution at different filling stages

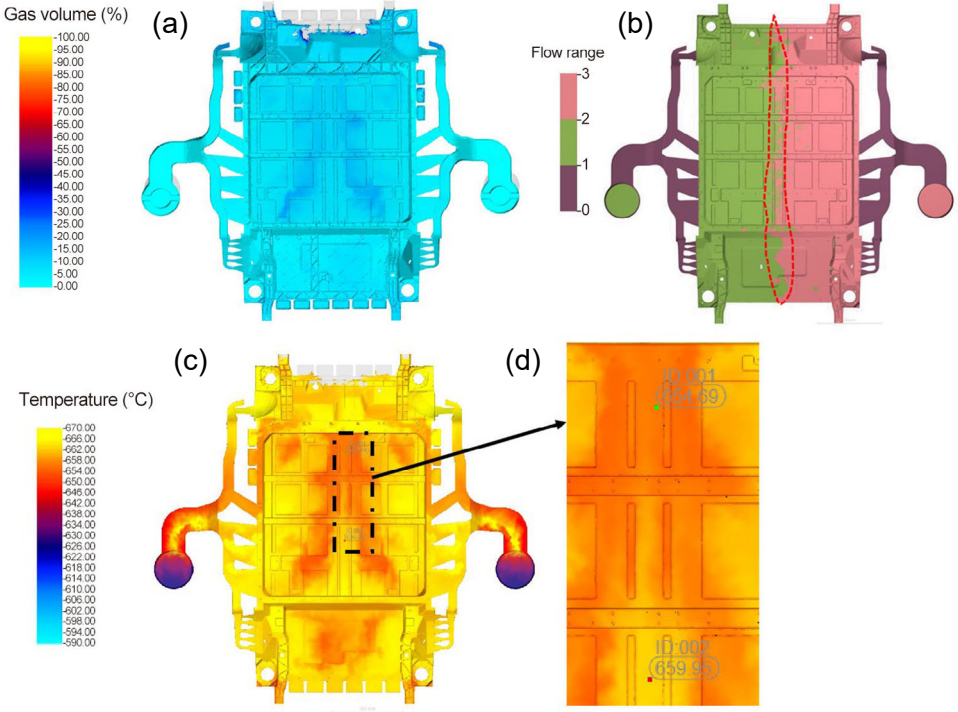

Fig. 13: Defects prediction of actual model: (a) gas content of mental liquid; (b) convergence area of mental liquid; (c) and (d) temperature field distribution in the final filling stage

rates are nearly consistent on both sides. The convergence occurs along the central region of the product, which is advantageous for shortening the pathway, and for maintaining a higher temperature of liquid metal in the final filling stage. As shown in Fig. 13(c), the temperature of the liquid metal varies during the final filling process, with the lowest temperature recorded in the central zone. Furthermore, the temperature of the molten metal remains above 650 °C, preventing the cold shuts and misruns in the actual product.

4.2.2 Effect of asynchrony in die-casting machine on production stability

On the production floor, the response time of the dual injection system may exhibit variability. For large-scale integrated die-casting products, the total filling duration falls within the range of 80–100 ms. Generally, the operation of the dual-sleeve injection can be managed within 5 ms. To evaluate the viability of asynchronous filling by dual punches, simulations were performed for scenarios with a 20 ms discrepancy between the

start and end times of the two punches.

Figure 14(a) illustrates the velocity field distribution as the liquid metal first enters the product. The left punch has achieved a high speed of 5.5 $m \cdot s^{-1}$, while the right punch is still in the initial acceleration stage, leading to a 20 ms difference times between the two sides. The velocity at the left gate runner begins to increase, with speeds exceeding 10 $m \cdot s^{-1}$ in the central region, as indicated by the red circled area in Fig. 14(a).

In contrast, due to the right punch not yet reaching a high speed, the velocity of the gate runner remains under 2 $m \cdot s^{-1}$. As shown in Fig. 14(b), despite the different speeds from the two sides, both sides of the flow area maintain symmetry during the asynchronous filling process by two punches.

Figure 15 illustrates the flow area where the liquid metal enters the product and the final convergence location. Despite a 20 ms disparity in the initiation speeds, the convergence zone of molten metal remains in the central area of the product. Notable, there is a minor deviation in specific locations from synchronous filling. Figure 15(a) presents the flow area of the liquid metal within the front cabin of the product during asynchronous filling. Due to the earlier initiation of the high speed on the left side, the flow range of molten metal is farther. However, the variance in flow range compared to synchronous filling is minimal, not exceeding 20 mm.

Similar to the flow range of the front cabin, the convergence zone of liquid metal deviation from the middle of the product is also much less than 50 mm, as shown in Fig. 15(b). Additionally, compared to the front cabin and battery cabin, the convergence zone of the rear floor plate is significantly influenced by asynchronous filling. As indicated by the black arrows in Fig. 15(c), during asynchronous filling, the convergence zone deviates by approximately 120 mm from the product's center. Conversely, during synchronous filling, this deviation is roughly 30 mm. On the lower side of the product, this variance remains within 100 mm.

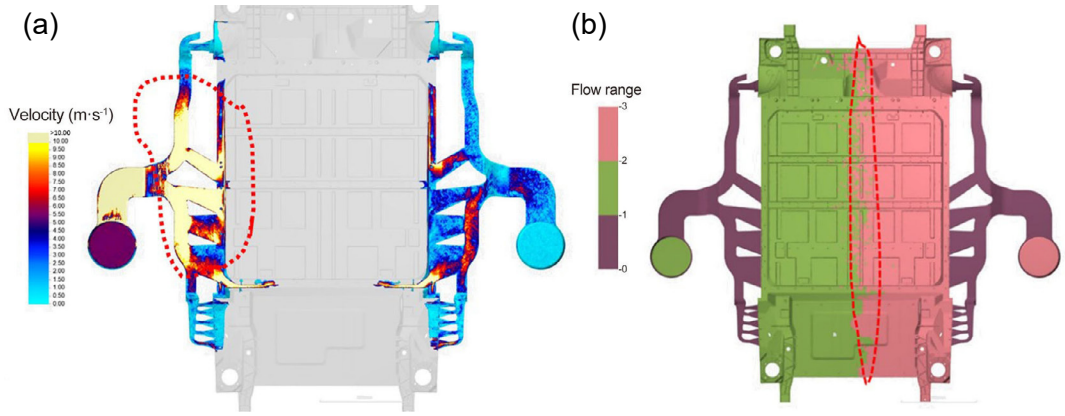

Fig. 14: Asynchronous simulation results: (a) velocity field distribution at high-speed completion stage and (b) liquid metal distribution in different injection systems

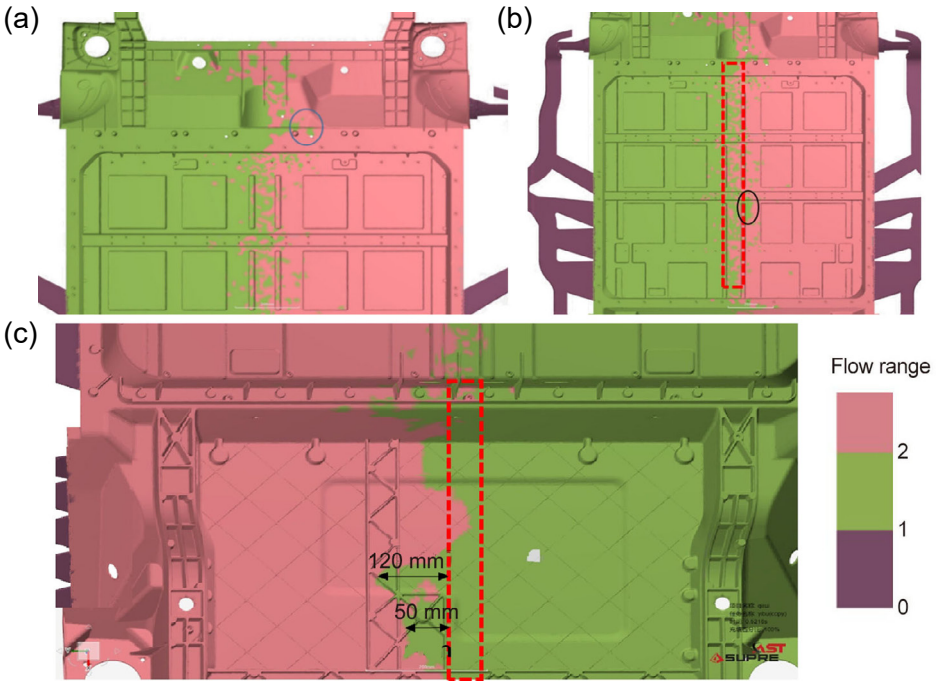

Fig. 15: Convergence results of asynchronous simulation: (a) front structure; (b) battery cabin; (c) rear floor

Through the simulation of synchronous and asynchronous filling with dual punches, the following conclusions are given: When the timing deviation is within 20 ms, the convergence area of the molten metal remains unchanged. A 20 ms difference between asynchronous and synchronous filling slightly alters the convergence zone, with the shift direction favoring the side of the higher-speed injection system. However, the magnitude of this shift is less than 120 mm. Therefore, minor variations in this system can preserve the stability and consistency of the manufacturing process.

4.3 Feasibility discussion

The die-casting flow simulation of the scaled model has demonstrated its precision through comparison with filling experiments. This simulation provides valuable support for the mold design and production process of the integrated 10,000 t die casting, which utilizes a dual-sleeve system.

Based on the mold flow analysis of the actual model, several key findings have been obtained. Firstly, the current design of gating runners ensures a sequential filling process within the double sleeves, which is crucial for the expulsion of gases. Secondly, this design significantly shortens the pathway of the molten metal, as illustrated in Fig. 16. It is important to maintain a higher temperature of liquid metal at the end of the filling stage, while avoiding defects such as cold shuts and misruns. Thirdly, despite the complexity of the asynchronous filling and dual injection system, the die-casting machine could reach precision control within 5 ms, ensuring the stability of production.

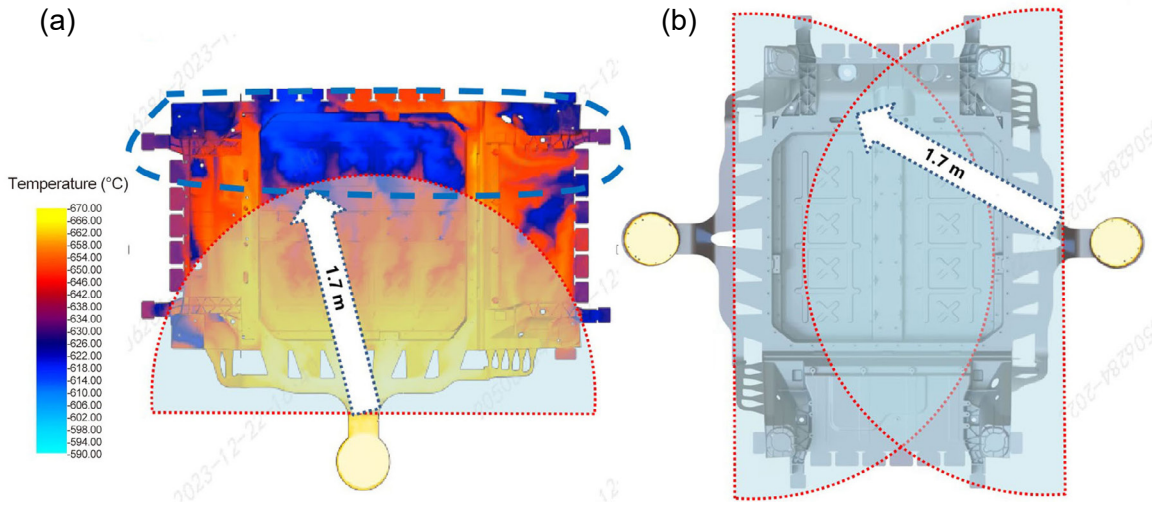

Fig. 16: Comparison of pathway in two gating systems: (a) temperature field of liquid metal at the end of the filling stage in a single-sleeve system; (b) flow range of a double-sleeve system

5 Conclusion

A feasible solution to produce the integrated car underbody with dual die casting injection systems was proposed. Firstly, a scaled model was utilized for analyzing the filling process of liquid metal and defects. Then, the simulation results and the actual filling results were compared for verifying the accuracy of simulation model. Finally, analysis was carried out on the actual model for exploring the feasibility, such as reduction of cold shut defects and decrease in metal flow length. Simulation results indicate that the dual-injection system can substantially decrease filling time and minimize cold shut defects. Both simulation and experimental data reveal that each injection system supplies molten metal to occupy half of the product area, significantly reducing metal flow length compared to a single-sleeve system. For a product with dimensions of 2,500 mm×1,300 mm, the flow length of the metal liquid could be kept under 1,700 mm. In the simulation of the actual model, the liquid metal from both sides of the gating system undergoes a high-speed filling stage. The flow sequence and filling process are very close to those observed in the scaled model. Furthermore, this ideal filling sequence facilitates the gas removal. When the injection systems of the die-casting machine are controlled asynchronously with a 20 ms time difference in the high-speed finished position of the metal liquid between the two injection systems, the overall convergence position of the metal liquid remains basically consistent and the convergence position of local area difference is less than 100 mm. However, the magnitude of this shift is less than 120 mm.

Acknowledgments

This work was supported by the National Natural Science Foundation of China (No. 52175284), and the National Key Research and Development Program of China (Grant No. 2022YFB3404201).

Conflict of interest

The authors declare that they have no known competing financial interests or personal relationships that could have appeared to influence the work reported in this paper.

References

[1] Codd D. Advanced lightweight materials development and technology for increasing vehicle efficiency. KVA Inc, Escondido, CA 92029, USA, 2008.
[2] Zhong Q, Yi S, Liu B. The application of aluminum alloy in automobile lightweight. Advanced Materials Industry, 2015, 2: 23–27. (In Chinese)
[3] Qiao X, Yang L, Liu S Y. Research on the development and application of integrated die casting technology. Auto Manufacturing Engineer, 2023, 08: 30–33, 52. (In Chinese)
[4] Baser T, Elif U, and Akinci V. New trends in aluminum die casting alloys for automotive applications. The Eurasia Proceedings of Science Technology Engineering and Mathematics, 2022, 21: 79–87.
[5] Wärmefjord K, Hansen J, and Söderberg R. Challenges in geometry assurance of megacasting in the automotive industry. Journal of Computing and Information Science in Engineering, 2023, 23(6): 060801.
[6] Naor M. Tesla's circular economy strategy to recycle, reduce, reuse, repurpose and recover batteries. Recycling-Recent Advances, IntechOpen, 2022.
[7] Lehmhus D. Advances in metal casting technology: A review of state of the art, challenges and trends – Part I: Changing markets, changing products. Metals, 2022: 1959.
[8] Rakoto B, and Ling L. 2022 Mega-casting trends for automotive manufacturers. White Paper, Ducker-Carlise, ed., 2022.
[9] Lijin Group. The world's first 16000T ultra large die-casting unit unveiled. Foundry Engineering, 2023, 47(6): 31–31. (In Chinese).
[10] Liu L, Cao G, Wang B, et al. The significance of integrated die-casting in new energy vehicles and quality control methods for die-casting. Forging & Stamping, 2023, 24: 19–23. (In Chinese)
[11] Li T, Song J, Zhang A, et al. Progress and prospects in Mg alloy super-sized high pressure die casting for automotive structural components. Journal of Magnesium and Alloys, 2023, 11(11): 4166–4180.
[12] Tesla Inc. Multi-directional unibody casting machine for a vehicle frame and associated methods. U.S. Patent No. 2019/0217380 A1, issued on July 18, 2019.
[13] Mega-casting trends for automotive manufacturers. https://www.linkedin.com/pulse/mega-casting-trends-automotive-manufacturers-2022-ducker worldwide/?trk=organization-update-content_share-article. June 6, 2023
[14] Janben C, Krafczyk M. Free surface flow simulations on GPGPUs using the LBM. Computers & Mathematics with Applications, 2011, 61(12): 3549–3563. https://doi.org/10.1016/j.camwa.2011.03.016.
[15] Körner C, Thies M, Hofmann T, et al. Lattice Boltzmann model for free surface flow for modeling foaming. Journal of Statistical Physics, 2005, 121: 179–196.
[16] Zhang A, Du J, Guo Z, et al. Conservative phase-field method with a parallel and adaptive-mesh-refinement technique for interface tracking. Physical Review: E, 2019, 100(2): 023305.
[17] Meng S, Zhang A, Guo Z, et al. Phase-field-lattice Boltzmann simulation of dendrite motion using an immersed boundary method. Computational Materials Science, 2020, 184: 109784.
[18] Shan X, Yuan X F, Chen H. Kinetic theory representation of hydrodynamics: A way beyond the Navier-Stokes equation. Journal of Fluid Mechanics, 2006, 550: 413–441.
[19] Zhang A, Guo Z P, Wang Q G, et al. Three-dimensional numerical simulation of bubble rising in viscous liquids: A conservative phase-field lattice-Boltzmann study. Physics of Fluids, 2019, 31(6). https://doi.org/10.1063/1.5096390
[20] Zhang X, Kang J, Guo Z, et al. Development of a Para-AMR algorithm for simulating dendrite growth under convection using a phase-field-lattice Boltzmann method. Computer Physics Communications, 2018, 223: 18–27.
[21] Ginzburg I, and Konrad S. Lattice Boltzmann model for free-surface flow and its application to filling process in casting. Journal of Computational Physics, 2003: 61–99. https://doi.org/10.1016/S0021-9991(02)00048-7
[22] Krüger T, Kusumaatmaja H, Kuzmin A, et al. The lattice Boltzmann method. Springer International Publishing, 2017: 4–15.
[23] Yu H, Luo L, and Girimaji S. LES of turbulent square jet flow using an MRT lattice Boltzmann model. Computers & Fluids, 2006: 957–965.
[24] Berger M, Rigoutsos I. An algorithm for point clustering and grid generation. IEEE Transactions on Systems, Man, and Cybernetics, 1991, 21(5): 1278–1286.
[25] Berger M, and Colella P. Local adaptive mesh refinement for shock hydrodynamics. Journal of Computational Physics, 1989, 82(1): 64–84.
[26] Ma K, Wang Y, Jiang M, et al. A simple one-step index algorithm for implementation of lattice Boltzmann method on GPU. Computer Physics Communications, 2023: 283.
[27] Futá P, Petrík J, Pribulová A, et al. The fluidity of Al-Si alloy: Computer simulation of the influence of temperature, composition, and pouring speed. Archives of Metallurgy and Materials, 2018, 63(4): 1799–1804.
[28] Niu Y, Zhao Y, Wang S, et al. Effects of Si content on casting fluidity, thermal conductivity and mechanical properties of Al-Mg-Si alloy. Foundry, 2016, 65(4): 3669–3705. (In Chinese).
[29] Luo N, Xu L. Metal die casting technology and mold design. Tsinghua University Press, 2006. (In Chinese)
[30] Pan X. Die casting technology and molds. Electronic Industry Press, 2006. (In Chinese)